Instrument Science Report WFC3 2021-13

Table-Based CTE Corrections for `flt`-Format WFC3/UVIS

Jay Anderson
August 13, 2021

ABSTRACT

The pixel-based CTE correction within the calwf3 pipleline has worked well for many years, but as the CTE-related losses continue to increase in low-to-moderate background images, the algorithm is no longer able to correct faint sources for CTE without inducing extreme amplification of readnoise. Thankfully, there are several ways available to correct for CTE losses in WFC3/UVIS images. The formula-based corrections are still effective for aperture photometry, but as a new photometry routine (`hst1pass`) is becoming available to measure images and correct photometric and astrometric measurements for CTE losses, we revisit these empirical corrections and put them into a format that is more useful for this application. To this end, we distill the corrections into simple 2-D tables that provides the photometric losses and astrometric shifts as a function of (1) the initial flux and (2) the local sky background. These tables have now been implemented into the soon-to-be-released `hst1pass` routine.

1. Introduction

This is a brief ISR that describes how we constructed the table-based CTE corrections for `flt`-format WFC3/UVIS images. These corrections were constructed from the standard set of CTE-calibration observations that are used to do CTE trending and formula-based corrections (see Kuhn & Anderson 2021).

The historical targets for these empirical CTE calibrations are 47 Tuc and NGC6791. The field in 47 Tuc is at an intermediate distance from the cluster center (6′). It has long served as a touchstone field for ACS and WFC3 photometric and astrometric calibration.

The other traditional CTE-monitor field in NGC6791 was chosen to ensure a low stellar density so that stars would never shield each other or otherwise interfere with the measurement of CTE losses. Over time, it was realized that the star density would have to be extremely high for such concerns to be important. And there was naturally a downside of such a sparse field: there were

not many stars in the field that could be used to probe the CTE losses. For this reason, in 2021 the WFC3 team decided to switch the sparse NGC6791 field to a denser field at the center of Omega Centauri. The core of Omega Centauri is large and not as concentrated as that of most clusters, so the star density is essentially constant within a HST field of view (3′×3′). Furthermore, Omega Cen's core density is almost perfect for providing a large number of stars without significant crowding, particularly if we want to focus on the lower part of the luminosity function.

In this document, we will focus on the recent Omega Cen observations taken with CAL-16401 (PI-Kuhn) and CAL-16441 (PI-Anderson). The CAL-16401 observations were taken with the standard strategy of taking an exposure of the field, then shifting the FOV up by one chip, so that the stars in the bottom chip in the first pointing are placed in the top chip in the second pointing. The fact that the two chips read out in opposite directions allows us to directly measure the photometric losses and astrometric shifts that are characteristic of CTE. Observations are also taken with a variety of post-flash levels so that we can directly calibrate CTE effects as a function of sky background.

This observing strategy has been used for many years to measure photometric losses, but it can also be used to measure astrometric losses. The same stars that have photometric losses also experience astrometric shifts. We will use this same dataset to calibrate the astrometric impact along with the photometric impact.

The photometric losses and astrometric shifts depend on several factors: (1) the number of parallel shifts, (2) the date of the observation, (3) the brightness of the source, and (4) the sky background. The first two dependencies are linear and easy to scale, but the latter two are non-linear. Our strategy will be to define a two-dimensional table to specify the losses as a function of source brightness and sky background. The table value can then be scaled up or down to account for different observation dates and numbers of parallel shifts.

This report is organized as follows. In **Section 2** we describe the observations that have gone into this report. In **Section 3** we discuss the need for a master list of stars. **Section 4** examines the photometric losses and **Section 5** the astrometric losses. **Section 6** details how these corrections have been folded into the `hst1pass` software package. Finally, **Section 7** ties it all together and suggests possible improvements for the future.

2. The Observations

This report will make use of two recent datasets. CAL-16401 (PI-Kuhn) was taken according to the standard CTE-monitor procedure, and CAL-16441 (PI-Anderson) was taken in a way that allowed us to focus on the faintest stars.

2.1 CAL-16401 (PI-Kuhn)

The first dataset comprised a two-orbit visit that straddled 2021 December 23-24. The first orbit had a single pointing centered on the cluster. The second orbit had a pointing that placed the top chip on the location of the bottom chip in the first pointing.

Table 1 shows the list of exposures. The background at the center of the cluster in F502N is about 0.04 electron per second. The combination of post-flash and natural background allowed us to probe the range of typical UVIS backgrounds (4 e^- to 29 e^-) roughly every 5 e^-. Even though a background of 20 e^- is recommended now, it is important to probe *all* backgrounds, both for legacy reasons and because different noise/mitigation compromises are possible in subarrays.

Table 1: List of observations for GO-16401.

POSTARG1	POSTARG2	FILTER	EXPTIME	POSTFLASH	OBSD BKGD
iegm01y1q	iegm01ysq	F502N	90 s	0 e^-	4 e^-
iegm01yaq	iegm01yfq	F502N	90 s	6 e^-	10 e^-
iegm01y2q	iegm01ygq	F502N	348 s	4 e^-	15 e^-
iegm01y4q	igem01yiq	F502N	348 s	8 e^-	19 e^-
iegm01y6q	iegm01ylq	F502N	348 s	12 e^-	24 e^-
iegm01y8q	igem01yqq	F502N	348 s	17 e^-	29 e^-

The GO-16401 images were analyzed with the software routine, `hst1pass`, which will be released shortly (see Anderson 2021). In brief, the routine goes through an flt/flc image pixel by pixel to determine which pixels may house stars. It subjects each pixel to a variety of finding criteria. The most basic criteria are HMIN and FMIN. A pixel may house a star if it is brighter than any of its neighbors within a radius of HMIN. Also, it may house a star if it has FMIN counts over sky within a radius of 1 pixel. The routine can also subject measured sources to quality-of-fit filters, but HMIN and FMIN are the most basic of the criteria. We adopted finding parameters **`HMIN=3`** and **`FMIN=25`**, so that we could include as many stars as possible. The stars would later be cross-identified with vetted star lists, so the reliability of sources in these lists was not critical.

Table 2: List of observations in program CAL-16441 (PI-Anderson).

OBSERVATION	FILTER	EXPTIME	POSTFLASH	OBSD BKGD
iehr02lhq	F606W	800 s	0 e^-	694 e^-
iehr02loq	F606W	800 s	0 e^-	694 e^-
iehr02lwq	F606W	800 s	0 e^-	694 e^-
iehr02m3q	F606W	800 s	0 e^-	694 e^-
iehr02ldq	F606W	4 s	6 e^-	12 e^-
iehr02lfq	F606W	4 s	8 e^-	14 e^-
iehr02lkq	F606W	4 s	10 e^-	17 e^-
iehr02lmq	F606W	4 s	12 e^-	19 e^-
iehr02lsq	F606W	4 s	15 e^-	22 e^-
iehr02luq	F606W	4 s	18 e^-	25 e^-
iehr02lzq	F606W	4 s	21 e^-	28 e^-
iehr02m1q	F606W	4 s	25 e^-	33 e^-

2.2 CAL-16441 (PI-Anderson)

The first dataset is focused on CTE corrections for stars that are bright enough to be found and measured in individual exposures. This means they need to be at least 5-sigma detections, since less significant detections require multiple independent observations to pin down their locations and validate them.

The CAL-16441 program was focused on fainter stars. We took four 800s exposures with no dither. By stacking these images, we were able to get a reliable model of the true astronomical scene. We also took eight 4s exposures with a variety of postflash levels. By comparing the surviving flux against the "truth" (the 800s stack, scaled down by a factor of 200 = 800/4), we could see the impact of CTE on the extremely low-signal stars at various background levels. **Table 2** lists the observations in CAL-16441.

This dataset was originally analyzed in WFC3 ISR 2021-09 by Anderson et al. We will incorporate many of their findings here.

3. The Need for a Master List

It is critical to start with a reliable list of stars when measuring CTE losses. This is because finding algorithms tend to find sources more often when they are brighter (i.e., more significant). This can result in a positive flux bias if we are not careful to start with an unbiased list. Also, it is good to start with a reliable flux for each star, since the fluxes we measure to assess CTE are only as reliable as the corrections we are trying to measure.

To get a list of reliable sources, we identified fifteen 60-s F606W exposures that were taken under CAL-15733 and CAL-16413 (for distortion calibration) at a variety of offsets and orientation in 2020 and 2021. We ran `hst1pass` on the `_flc` images and combined the individual source lists into a common master list, requiring a star to be found in at least 6

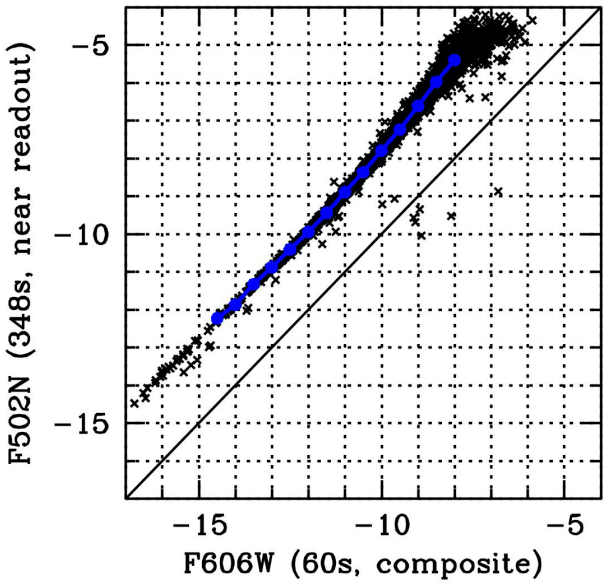

F606W (60s)	F502N (348s)
−14.50	−12.22
−14.00	−11.86
−13.50	−11.32
−13.00	−10.87
−12.50	−10.40
−12.00	−9.94
−11.50	−9.44
−11.00	−8.89
−10.50	−8.36
−10.00	−7.79
−9.50	−7.23
−9.00	−6.61
−8.50	−5.98
−8.00	−5.40

Figure 1: The instrumental flux as measured in the 60s F606W reference list against the 348s F502N flux for stars within ~200 transfers of the readout. The blue points show the fitted trend.

exposures. This process provided us with a list of 126,205 reliable stars with positions accurate to about 0.1 pixel in the ~2020.5 epoch. Stars in the core of Omega Cen have internal proper motions of about 1 mas/yr, which corresponds to about 0.025 WFC3/UVIS pixel per year. Since the reference epoch is within 6 months of the CAL-16401 observations, it is clear that internal motions should not affect our ability to make use of this master star list.

The master-list fluxes will be more important than the master-list positions. CTE flux losses are assessed for stars in bins of true flux and background sky. This is done by comparing the flux measurements for stars that are far from the readout register in one exposure against measurements for the same stars in another image where they are found close to the readout register. It is hard to sift stars into magnitude bins when the magnitudes we are using for sifting may themselves be impacted by CTE-related flux losses. For instance, stars in the middle of both images will both suffer CTE flux losses, so if we base our magnitude-binning on the apparent fluxes of stars, our bins will be shifted and non-uniform. This is why good master-list fluxes are important.

To get a reliable true F502N brightness for each star, we compared the 60-s F606W reference photometry against 348-s F502N photometry from image `iegm01y4q` (which had a background of 20 electrons). **Figure 1** shows the stars that are within 200 pixels of the readout (such that they should suffer minimal CTE losses). The table on the right of the figure directly relates the fluxes in the two bands. We can interpolate this table to map the catalog F606W photometry to an expected flux in a 348s exposure in F502N. This will allow us to properly bin the observations so that we can measure the CTE-related flux losses in a consistent way.

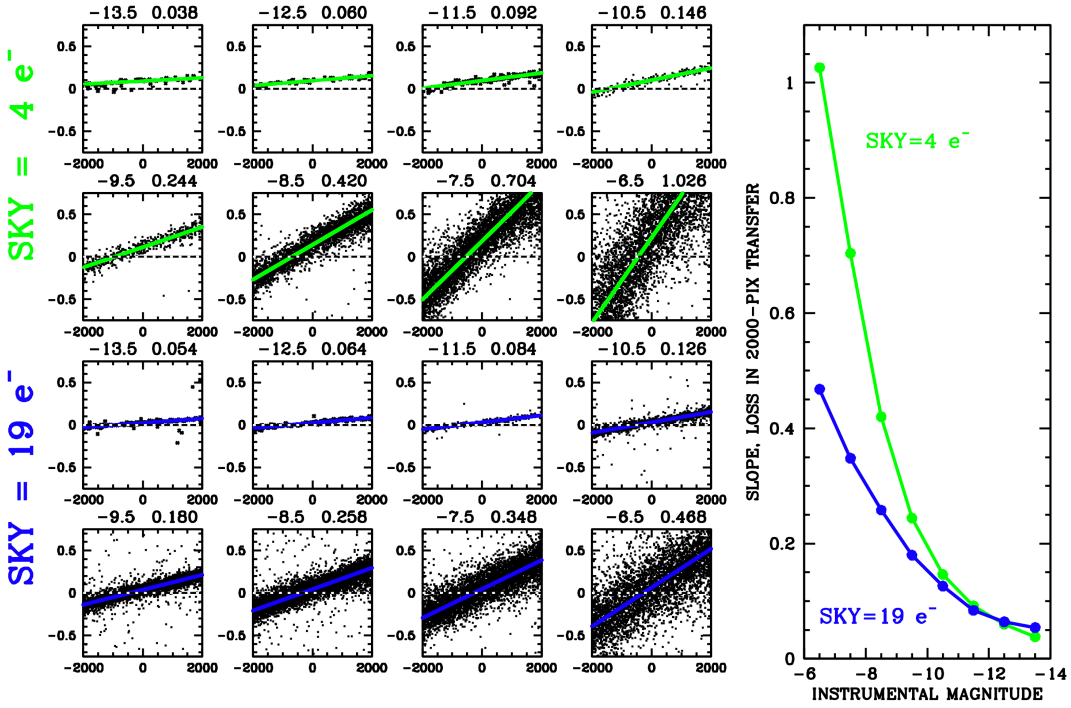

Figure 2: Each panel in the array on the left shows $\Delta m_{1\text{-}2}$ versus $\Delta j_{1\text{-}2}$ for a different magnitude bin (as labeled to the upper left of each panel). The slope is fitted to each and is reported at the upper right of each panel and plotted on top of the points. The top two rows (with the green trendlines) show the results for the sky = 4 e⁻ images (`iegm01y1q` and `iegm01y1q`) and the bottom two rows (with the blue trendlines) show the results for the sky = 19 e⁻ images (`iegm01y4q` and `iegm01yiq`). The CTE flux-loss slopes for the two pairs are shown in the composite plot (right).

4 Measuring the photometric trends

CTE photometric losses are proportional to the number of parallel transfers, j_{trans}, that the star undergoes to get to the readout register. If in image#1, the star undergoes j_1 transfers, and in image#2 it undergoes j_2 transfers, then the relative magnitude shift due to CTE will be $\Delta m_{12} \equiv (m_1 - m_2)$ and is proportional to $\Delta j_{12} \equiv (j_1 - j_2)$.

Figure 2 shows the Δm_{12} photometric trends as a function of Δj_{12} for the 4-e⁻ and 19-e⁻ background image pairs for eight bins of magnitude, from near central-pixel saturation at instrumental magnitude[1] $m = -13.5$ to much fainter at an instrumental magnitude of −6.5, where the central pixel flux is 80 e⁻. The slope in each panel is related to the per-transfer CTE losses for the stars in that bin at that background. The plot on the right distills all these measured slopes into a simple curve for the two background levels shown in the individual panels.

[1] An instrumental magnitude is simply $-2.5 \log_{10}$(flux), where the flux is in electrons.

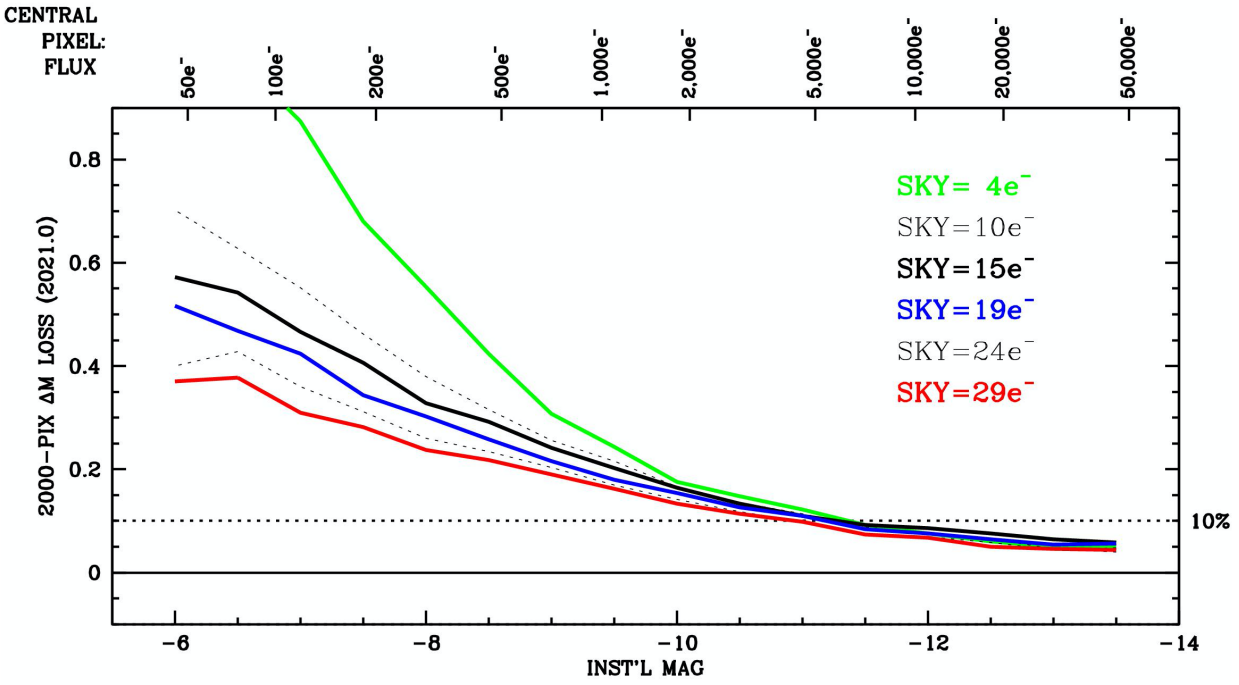

Figure 3: This plot adds to the left panel of Figure 2 the trends for all sky-background levels between ~5 electrons and ~30 electrons.

Note that in most of the panels there is a non-zero value for Δm_{12} at $\Delta j_{12} = 0$, i.e., at the chip centers where the two exposures should suffer the same CTE photometric losses. This is related to a simple zero-point shift between images. Such shifts tend to be ±0.02 magnitude or so and are related to changes in focus that affect the aperture correction for the 5×5-pixel aperture used by the software routine `hst1pass`. This offset is generally the same for all the panels for each image pair; the offset happened to be larger for the 4-e^- sky pair.

Figure 3 provides the CTE-related flux-loss trend as a function of true instrumental magnitude for sky background levels from ~5 electrons to ~30 electrons, the typical range of WFC3/UVIS observations. We distill this information into **Table 3**.

There is some noise in these trends, particularly at the bright end where there are not many stars to constrain the slope in the short 90-s F502N observations. So, we smooth out these trends and enforce them to be monotonic with flux and with background. In addition, we supplement these values at the faint end with the findings from GO-16441 as distilled in WFC3 ISR 2021-09 (Anderson et al.), which show what happens to extremely faint sources on various backgrounds. We found an offset of about 0.1 mag between the bottom row in **Table 3** and the results in Table 4 of WFC3 ISR 2021-09. We added this shift to the imported data and folded the new numbers into the table. The shift is likely due to the different apertures used (5×5 pixels here, and 2×2 pixels in the ISR).

Table 3: Raw measurement of CTE flux losses (in magnitudes) for stars with true instrumental magnitude listed on the left, and the sky listed in the column head, after 2000 pixels of parallel transfer. These are the raw fitted values. Tables 4 and 7 make improvements on these values.

TRUE	SKY BACKGROUND					
m_{inst}	4 e^-	10 e^-	15 e^-	19 e^-	24 e^-	29 e^-
–13.5	0.038	0.040	0.058	0.054	0.048	0.044
–13.0	0.050	0.046	0.064	0.054	0.046	0.046
–12.5	0.060	0.066	0.076	0.062	0.058	0.048
–12.0	0.082	0.072	0.086	0.078	0.070	0.068
–11.5	0.092	0.088	0.092	0.082	0.076	0.074
–11.0	0.120	0.114	0.110	0.110	0.098	0.096
–10.5	0.144	0.134	0.134	0.126	0.116	0.114
–10.0	0.172	0.166	0.164	0.154	0.142	0.132
–9.5	0.246	0.216	0.202	0.180	0.170	0.162
–9.0	0.304	0.256	0.242	0.218	0.204	0.190
–8.5	0.426	0.316	0.292	0.256	0.234	0.220
–8.0	0.532	0.380	0.324	0.302	0.262	0.236
–7.5	0.698	0.460	0.398	0.344	0.312	0.284
–7.0	0.882	0.548	0.464	0.424	0.352	0.304
–6.5	1.048	0.642	0.540	0.468	0.432	0.370

Table 4 reports our best measurement for the photometric loss in magnitudes, as a function of the star's true flux and the sky background, for stars that were located 2000 pixels from the serial register and measured in a 5×5-pixel aperture. The values that have been smoothed are shown in green and the values supplemented at the faint end are shown in blue.

The entries in this table vary smoothly, so to determine a value at an intermediate location, one can simply use linear interpolation. The table shows the losses for a star at $j = 2000$. If the star is closer to the readout register, one should multiply the table entry by $f_j = (j/2000)$, since losses are linear with the number of transfers. Similarly, the table was constructed from observations taken in 2020.98. For observations taken at a different date, one should multiply the table entry by $f_d = (d–2009.4)/(2020.98–2009.4)$. CTE flux losses generally increase linearly with the time, as the detector suffers increasing radiation damage the longer it stays in the harsh environment of space.

Finally, it is important to note that this table quantifies losses as a function of *true* flux, not observed flux. It is not possible to tabulate the data as a function of *observed* flux, since we would have to come up with a different table for different numbers of parallel transfers and different observation dates. To determine the "true" flux from an observation flux will require some iteration, which we describe in **Section 6**.

Table 4: CTE flux losses (in magnitudes) for stars with true instrumental magnitude listed on the left, and the sky listed in the column head, after 2000 pixels of parallel transfer, corresponding to the 2020.98 epoch. See text for an explanation of the colors. This table is superseded by Table 7.

TRUE m_{inst}	SKY BACKGROUND					
	4 e^-	10 e^-	15 e^-	19 e^-	24 e^-	29 e^-
–13.5	**0.054**	**0.052**	**0.050**	**0.048**	**0.046**	0.044
–13.0	**0.063**	**0.060**	**0.057**	0.054	**0.050**	0.046
–12.5	**0.072**	**0.068**	**0.064**	0.062	0.058	0.048
–12.0	0.082	**0.084**	0.086	0.078	0.070	0.068
–11.5	0.092	**0.092**	**0.088**	0.082	0.076	0.074
–11.0	0.120	0.114	0.110	0.110	0.098	0.096
–10.5	0.144	0.134	0.134	0.126	0.116	0.114
–10.0	0.172	0.166	0.164	0.154	0.142	0.132
–9.5	0.246	0.216	0.202	0.180	0.170	0.162
–9.0	0.304	0.256	0.242	0.218	0.204	0.190
–8.5	0.426	0.316	0.292	0.256	0.234	0.220
–8.0	0.532	0.380	0.324	0.302	0.262	0.236
–7.5	0.698	0.460	0.398	0.344	0.312	0.284
–7.0	0.882	0.548	0.464	0.424	0.352	0.304
–6.5	1.048	0.642	0.540	0.468	0.432	0.370
-6.0	1.120	0.701	**0.600**	**0.512**	**0.465**	**0.390**
–5.5	1.160	0.760	**0.660**	**0.556**	**0.489**	**0.410**
–5.0	1.260	0.860	**0.760**	**0.633**	**0.540**	**0.435**
–4.5	1.360	0.960	**0.860**	**0.710**	**0.577**	**0.461**
–4.0	1.710	1.310	**1.110**	**0.889**	**0.709**	**0.490**
–3.5	2.000	1.660	**1.560**	**1.068**	**0.841**	**0.513**

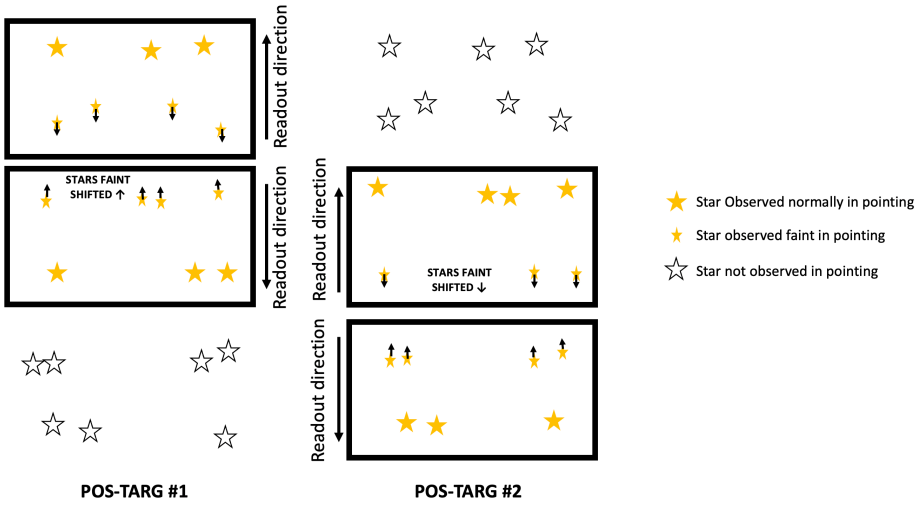

Figure 4: Schematic showing the two vertically shifted observations of the same star field, which for the purposes of this illustration have stars of all the same intrinsic brightness. The two POS-TARG pointings both observe the middle part of the field, with imperfect CTE affecting the stars in different ways in the different observations. Imperfect CTE causes stars that are farther from the readout register to be observed fainter and shifted away from the readout register (toward the gap).

5 Measuring the astrometric trends

In addition to photometric losses, it has been known since Kozhurina-Platais (2007, KP07) that CTE degradation causes astrometric shifts as well. As the pixels of a star are shifted down the detector, the electrons in the pixels at the leading edge of the star profile are more likely to be trapped than those on the trailing edge. Similarly, it is more likely that the charge trapped from the leading edge will be deposited on the trailing edge. Both of these effects tend to shift the apparent position of the star upwards, away from the direction of parallel readout (and towards the chip gap). As shown in KP07, the fainter stars will experience more of a shift than the brighter stars.

5.1 Observing the astrometric trends

The same chip-shifted dataset that can be used to measure photometric losses can be used to measure astrometric shifts as well. The shifts in position go hand-in-hand with the photometric losses, so instead of comparing $\Delta m_{1\text{-}2}$ against $\Delta j_{1\text{-}2}$, we can compare $\Delta y_{1\text{-}2}$ against $\Delta j_{1\text{-}2}$. The shifts we are measuring are illustrated in **Figure 4**.

Comparing positions, though, is slightly more complicated than comparing fluxes. HST cannot execute POS-TARGs perfectly and, even if it could, the distortion solutions are different for the two chips, so the astrometric comparison will necessarily be more involved. Also, breathing can introduce non-linear changes that can mimic the CTE-related shifts. For all these reasons, we must define a frame of reference that is local to the exposures. We will use the stars in the brightest magnitude bin (those between instrumental magnitudes −14 and −13) to define a transformation from the second pointing to the first. Then we can observe by how much the fainter stars shift with respect to this bright network.

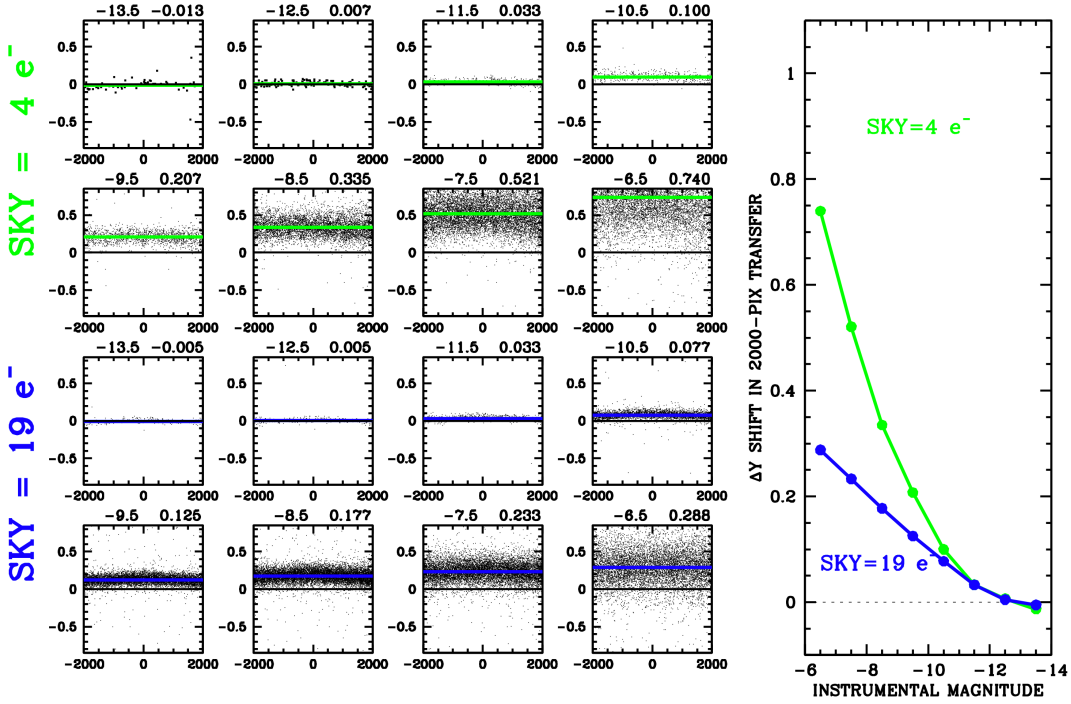

Figure 5: Similar to Figure 2, but here we show $\Delta y_{1\text{-}2}$ as a function of $\Delta j_{1\text{-}2}$ for bins of true instrumental magnitude for the same two backgrounds. We show the fitted levels visually in blue/green on each plot and list the fitted value to the upper right of each plot. On the right, we show the trends against instrumental magnitude.

To measure the astrometric shifts, we first cross-identify the stars common to the two exposures, using the same master list we used before for photometry. We then define a linear transformation based on the distortion-corrected positions of the brightest stars in the two frames:

$$\begin{pmatrix} U \\ V \end{pmatrix} = \begin{bmatrix} A & B \\ C & D \end{bmatrix} \begin{pmatrix} X - X_0 \\ Y - Y_0 \end{pmatrix} + \begin{pmatrix} U_0 \\ V_0 \end{pmatrix},$$

Where X and Y are the distortion-corrected positions in the first frame and U and V are the distortion-corrected positions in the second frame. It may look like there are 8 free parameters here, but one of the offsets, say, (X_0, Y_0) is arbitrary, so there are actually only six to solve for. These are solved for with least squares based on the associated positions of the list of N stars: (X_n,Y_n) and (U_n,V_n). If we set (X_0, Y_0) to be the centroid of the positions in the first frame, then the least-squares solution for (U_0, V_0) is the centroid of the positions in the second frame. This leaves us the linear terms A, B, C, and D, and there exist simple least-squares formulae to solve for them based on the coordinate pairs of the associated stars.

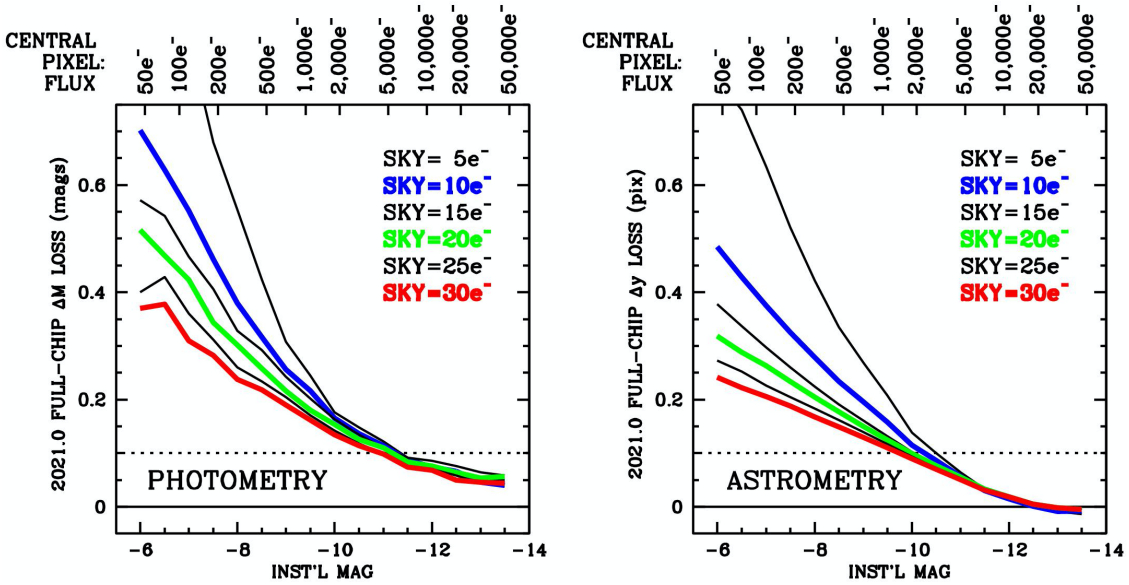

Figure 6: On the left we reproduce Figure 3, which shows the CTE-loss trends against star brightness for 6 different sky background levels. On the right we show the same figure for the astrometric shifts.

It is worth noting that the distortion-corrected frame that we have adopted, (X, Y), has an orientation and a scale that are very similar to those of the distorted frame (x, y). Therefore, the offsets we measure in that frame will be directly comparable to offsets in the undistorted frame. **Figure 5** provides the astrometric equivalent to **Figure 2**, which was for photometry.

The relationship between $\Delta m_{1\text{-}2}$ and $\Delta j_{1\text{-}2}$ is different from that between $\Delta y_{1\text{-}2}$ and $\Delta j_{1\text{-}2}$. With magnitude, a star goes from being brighter in one image at the bottom edge of the field, and brighter in the other image at the top of the field. This results in a trend in $\Delta m_{1\text{-}2}$ from negative to positive as in $\Delta j_{1\text{-}2}$ goes from –2000 to +2000. With astrometry, the $\Delta y_{1\text{-}2}$ shift is always in the same direction with the same amplitude (at a given true flux and for a field offset of 2000 pixels). This is because the Δy shift has a different direction in the different chips, since the parallel shifts move the charge in opposite directions. The Δm shift is in the same direction (negative) for both detectors.

To measure the astrometric residual, we compare where a star appeared to be in image #1 against where image #2 said the star should have been in image #1 (as computed by means of the transformations based on the positions of the bright stars in both images). **Figure 4** shows us that if we examine $\Delta y_{1\text{-}2} = y_1 - y_2$ as a function of y location, then at the top of the common field, y_1 has an apparent shift upwards, but at the bottom of the field, y_2 has an apparent shift downward. In the middle, y_1 has a moderate shift up and y_2 a moderate shift down. The difference y_2-y_1 is always about the same, consistent with **Figure 5**.

The right panel of **Figure 6** shows the astrometric-shift residuals for the six sky backgrounds. The photometric losses are shown on the left, for comparison. It is interesting that the scale of the losses and shifts are very similar, even though their units are very different (magnitudes and pixels). This is because a change of 0.01 magnitude corresponds to a 1% change in flux, and

since the FWHM is on the order of a pixel, a shift of 1% of the flux will introduce a ~0.01-pixel shift.

Note also that the astrometric shifts go to zero at instrumental magnitude of about −13, even though the plot on the left shows that there are still significant CTE losses for these bright but unsaturated stars. This is an artifact of the fact that, in order to measure the astrometric shifts, we had to transform the positions into a common frame, and we had to use the bright stars to do this. As mentioned before, any shifts in the bright stars are absorbed into the transformations and will not show up as residuals. In essence, we are measuring the shifts for the fainter stars relative to the shifts of the brighter stars. We can will correct for this this below. **Table 5** documents the raw shifts shown in the right panel of **Figure 6**.

Table 5: Raw measurement of Δ*y* astrometric CTE shifts (in pixels) after 2000 pixels of parallel transfer at epoch 2020.98, for stars with true instrumental magnitude listed on the left and with sky values listed in the column head. These are the raw values from direct fits to the residuals. Table 6 will improve these table values, and Table 8 will contain the final values.

TRUE m_{inst}	ASTROMETRIC SHIFT (Δ*y*, in pixels)					
	4 e^-	10 e^-	15 e^-	19 e^-	24 e^-	29 e^-
−13.5	−0.013	−0.008	−0.006	−0.005	−0.006	−0.005
−13.0	−0.009	−0.009	−0.003	−0.002	−0.002	−0.002
−12.5	0.007	0.001	0.005	0.005	0.004	0.005
−12.0	0.018	0.015	0.019	0.019	0.017	0.018
−11.5	0.033	0.030	0.033	0.033	0.032	0.032
−11.0	0.064	0.056	0.056	0.056	0.053	0.051
−10.5	0.100	0.087	0.079	0.077	0.072	0.070
−10.0	0.139	0.115	0.102	0.099	0.093	0.089
−9.5	0.207	0.158	0.132	0.125	0.116	0.110
−9.0	0.268	0.196	0.161	0.150	0.139	0.130
−8.5	0.335	0.234	0.191	0.177	0.161	0.149
−8.0	0.422	0.279	0.224	0.204	0.183	0.168
−7.5	0.521	0.326	0.260	0.233	0.205	0.188
−7.0	0.634	0.375	0.297	0.263	0.226	0.205
−6.5	0.740	0.429	0.337	0.288	0.252	0.222
−6.0	0.800	0.485	0.378	0.318	0.272	0.241

5.2 Measuring shifts for the bright stars

The only way to measure the bright-star shifts is to bring in some additional information. **Figure 7** illustrates how one can measure them from a complementary dataset. If we can find an observation that overlaps the gap (such as the light-green-shaded chip in the illustration), then we can use it to tell us the true positions of the stars on the two sides of the gap, and we can use that to measure the Δ*y* shift across the gap.

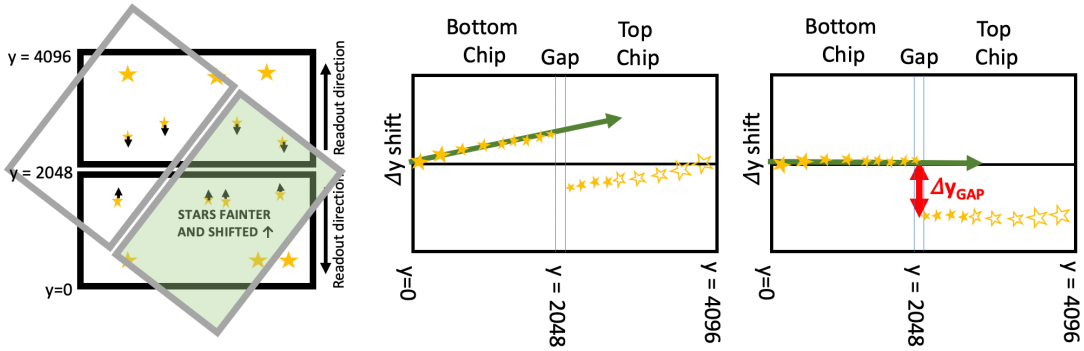

Figure 7: (Left) The observation in heavy black has stars with CTE shifts. The stars near the gap are fainter and shifted towards the gap relative to the stars closer to the serial registers (at $y = 0$ and $y = 4096$). (Middle) This shows the Δy shift as a function of y coordinate in an abutted system. The heavy green arrow shows the fit of bottom-chip coordinate system to the overlapping shaded green chip. (Right) The top-chip residuals relative to the positions inferred from the overlapping chip. The measurement Δy_{GAP} corresponds to 2× the CTE shift at the top of the detector for this brightness of star.

All we need here is to measure the gap-shift for the brightest stars (in the top magnitude bin), so we sought an overlapping frame that could give us good positions for those stars. Since stars at the center of Omega Cen move by 1 mas/yr (0.025 WFC3/UVIS pix/yr), as mentioned above, we were mindful to search for an overlapping frame at the same epoch. We found many overlapping images in the archive, but very few were shallow enough to ensure that the bright stars in our F502N images would be unsaturated (and hence measured well in the comparison images).

The only images we found that could help us were taken with WFC3/IR. The star positions in these images are not as accurate as the positions in WFC3/UVIS, on account of the larger pixels (120-mas pixels in WFC3/IR compared to the 40-mas WFC3/UVIS pixels). But since the goal was simply to measure a bulk shift, the WFC3/IR images should be adequate.

We are focused here on the brightest stars. The advantage of working with a narrow magnitude range of stars is that when we do a linear fit between the coordinate system of the comparison frame and that of the bottom chip, the linear nature of transformation should naturally absorb any CTE-related shifts in either the target frame or the comparison frame. We can then observe the chip gap without complications by examining how the extrapolated positions of the comparison frame compare with the observed positions in the top frame. The gap-shift measured corresponds to twice the shift at the top of either chip. **Figure 8** shows the shift across the chip-gap for four different sky backgrounds.

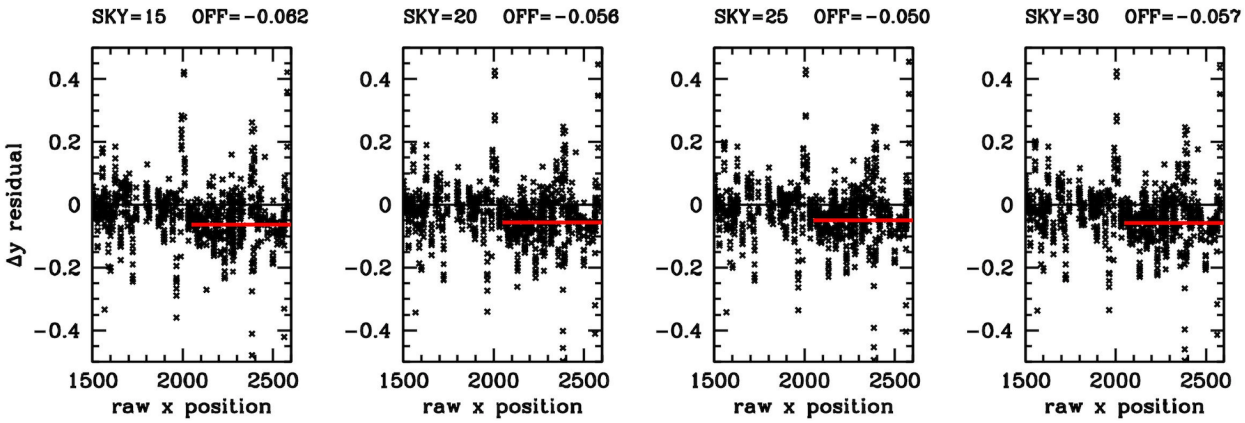

Figure 8: The shift across the chip-gap as measured with the stars in the brightest magnitude bin in the four 348s observations against WFC3/IR images.

We thus were able to fill in the orange values at the top of **Table 6**. The green values were smoothed relative to the original **Table 5**.

Note the astrometric table doesn't go as faint as the photometric table goes. It is easier to measure fluxes than positions for super-faint stars, since for photometry one can use fixed positions from stacks and measure whatever flux lands within a fixed aperture. To measure positions, it is necessary to have a clear peak in each exposure. When extrapolating this table to sky values outside of bounds of the table, we will just assume the table continues with the value at the edges. In the future, it will be good to extend the table, both to sky valued below 4 electrons and above 30 electrons.

Table 6: The same as Table 5, except that we have added the orange values to the table in the top magnitude bin using data from Figure 8. The values in the fainter bins have been adjusted upward accordingly. As with Table 5, the green values correspond to smoothed/extrapolated values. See Table 8 for the final version of this table.

TRUE m_{inst}	ASTROMETRIC SHIFT (Δ*y*, in pixels)					
	4 e^-	10 e^-	15 e^-	19 e^-	24 e^-	29 e^-
−13.5	0.035	0.033	**0.031**	**0.029**	**0.027**	**0.025**
−13.0	0.028	0.036	0.034	0.032	0.031	0.018
−12.5	0.046	0.043	0.041	0.039	0.037	0.035
−12.0	0.058	0.056	0.054	0.052	0.050	0.048
−11.5	0.073	0.071	0.069	0.067	0.065	0.062
−11.0	0.102	0.096	0.094	0.090	0.086	0.081
−10.5	0.123	0.117	0.114	0.111	0.105	0.100
−10.0	0.168	0.143	0.135	0.133	0.126	0.119
−9.5	0.236	0.186	0.167	0.159	0.149	0.140
−9.0	0.297	0.224	0.196	0.184	0.172	0.160
−8.5	0.364	0.262	0.226	0.211	0.194	0.179
−8.0	0.451	0.307	0.259	0.238	0.216	0.198
−7.5	0.550	0.354	0.295	0.277	0.238	0.218
−7.0	0.663	0.403	0.332	0.297	0.259	0.235
−6.5	0.769	0.457	0.372	0.322	0.285	0.252
−6.0	0.829	0.513	0.413	0.352	0.305	0.271

6 Software implementation of the table-based corrections

It was noted at the end of **Section 4** that using the table-based corrections would require iteration. Since the vertical axis of the table is true flux and we start only with the observed flux (which includes the unknown CTE flux loss), we must iterate to find the correction to give us the true flux.

6.1 The iterative process

In the process of measuring each star, we produce a sky value, typically by finding the robust mean of the star-subtracted pixels in an annulus between 6- and 9-pixels' radius. In the `_flt` images produced by the pipeline, the `_flt` image has had the dark current and the post-flash subtracted. In order to determine the actual background that the star was transferred upon, we add back in the dark current and the post-flash. (Alternatively, one could run the pipeline without dark or post-flash subtraction, but the result is equivalent.)

Once we have a value for the sky background for each star, we interpolate the photometric and astrometric correction tables at the particular sky value appropriate for this star, i.e., along a vertical line through the table. We then scale these corrections by f_d and f_j, where $f_d = (d–2009.4)/(2020.98–2009.4)$ and $f_j = (j/2000)$ and d is the date in fractional years and j is the number of parallel shifts to the readout register. This gives us a pair of simple functions, $\Delta m(m_{\rm true})$ and $\Delta y(m_{\rm true})$, tabulated at values of $m_{\rm true}$ from –13.5 to –6.0. This is essentially a vertical line through the table. We can linearly interpolate these smooth 1-D tabulated functions to get intermediate values.

We now start the iterations by adopting the observed flux as the first estimate of the true flux: $m_{\rm true}^{[0]} = m_{\rm obs}$. We then interpolate $\Delta m(m_{\rm true}^{[0]})$ to determine the first correction to the photometry $\Delta m^{[0]}$. For the first iteration, we set $m_{\rm true}^{[1]} = m_{\rm obs} - \Delta m^{[0]}$ and evaluate $\Delta m^{[1]}$ at $m_{\rm true}$. We then re-determine $m_{\rm true}^{[2]} = m_{\rm obs} - \Delta m^{[1]}$ and stop when $\Delta m_{\rm true}^{[N]}$ is arbitrarily close to $\Delta m^{[N–1]}$. The final value for $m_{\rm true}$ is then determined to be $m_{\rm true} = m_{\rm obs} - \Delta m^{[N]}$.

Once we have a value for $m_{\rm true}$, we solve for $y_{\rm true} = y_{\rm obs} - \Delta y(m_{\rm true})$, keeping in mind that the y shift is always in the direction away from the amplifier. In other words, it is in the direction of the gap for both the bottom chip and the top chip.

6.2 Software implementation

This iterative procedure has been implemented within the `hst1pass` software program, which is currently being prepared for release, along with some documentation (see Anderson 2021). As its name suggests, the routine does one-pass photometry on HST images (specifically WFPC2, ACS and WFC3 observations). This means that it measures stars under the presumption that they are isolated enough to ignore their neighbors. Most stars in HST images are well-suited for this treatment, particularly when one uses a small aperture — `hst1pass`'s default aperture is 5×5 pixels.

When using such a small aperture, it is important to have a good handle on the PSF. The routine `hst1pass` makes use of a large library of empirical PSFs extracted from calibration images that are designed to have a good distribution of high signal-to-noise stars. These PSFs allow positions to be measured to better than 0.02-pixel (RMS) and fluxes to be measured to better

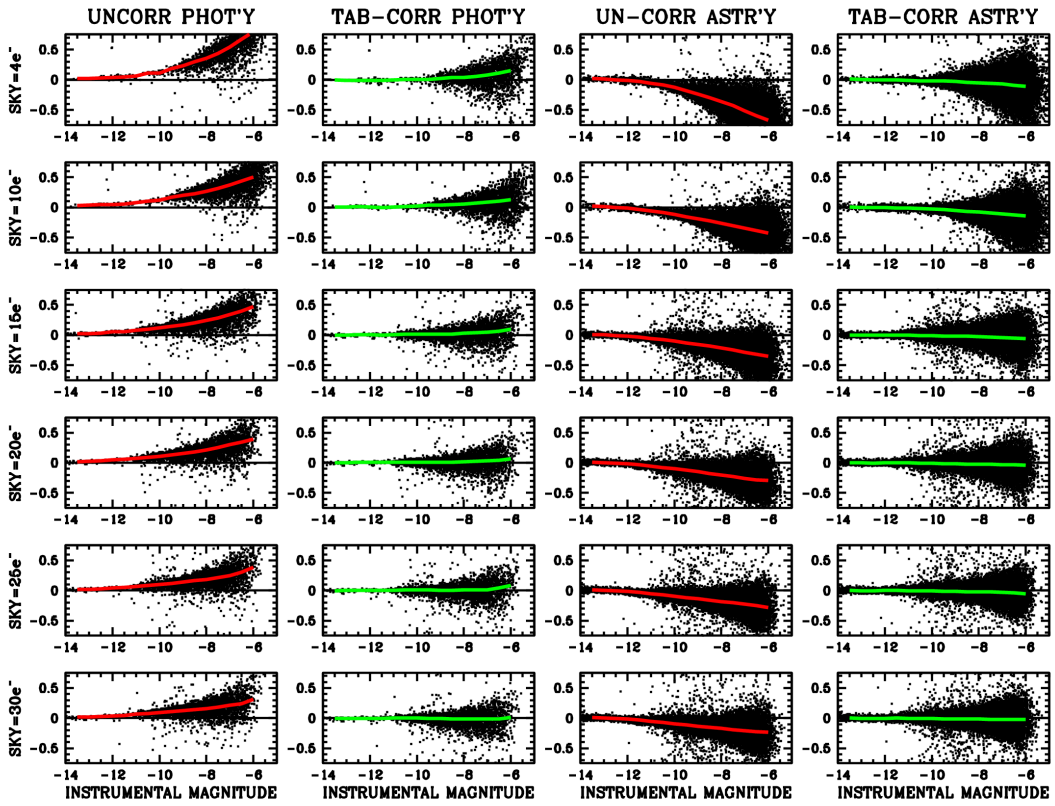

Figure 9: Results of a re-analysis of the CAL-16401 data from Omega Centauri. The plots with the red trendlines show the uncorrected results and those with the green trendlines show corrected results based on the Tables 4 and 6. Photometric residuals are shown in the left two columns, and astrometric residuals in the right two columns. The rows correspond to different sky levels, as labeled on the left.

than 0.01 magnitude (RMS), when the star has adequate signal-to-noise. With the prescriptions provided here, the photometry and astrometry can be corrected for any CTE-related biases.

When the `hst1pass` routine encounters a WFC3/UVIS `_flt` image, it automatically implements the table correction and outputs the CTE-corrected *y* position and CTE-corrected instrumental magnitude *m*, by default. One can also access the uncorrected values as well to examine the correction.

6.3 Validation

We ran the `hst1pass` routine on the CAL-16401 images analyzed in **Sections 4** and **5**. **Figure 9** shows the astrometric and photometric results. The photometric comparisons shown here are made at the top of the detector relative to the center, and the astrometric comparisons shown are relative to the brightest stars.

Note that there are some small remaining trends in the green curves. This is not surprising, as the sky values used in the tables were taken from the whole-image background. Postflash is not uniform across the entire image and there can be slight differences in the background. Furthermore, stars were not always uniformly distributed in the magnitude bins, which can introduce slight biases in the determined table values.

To improve this, we added the residuals in the green curves above to the tables to improve the correction one final time. The final tables are provided below and are what will be used in the official release of `hst1pass`. We re-examined the residuals shown in **Figure 9** after implementing the values in the final tables (**Table 7** and **Table 8**). As we expected, the residuals improved; most were less than 0.01 magnitude in flux and 0.01 pixel in *y* position.

Finally, it is worth noting that the loss curves and shift curves in red exhibit very similar loss/shift trends in photometry/astrometry for sky levels 20 electrons and above. This provides additional confirmation that maintaining a minimum background of 20 electrons stems much of the CTE impact for the bright and moderately faint stars.

Table 7: The final table values for the photometric correction, $\Delta m(m_{true}, s)$, in magnitudes. Table values correspond to 2000 parallel shifts for epoch 2020.98.

TRUE	SKY BACKGROUND					
m_{inst}	4 e^-	10 e^-	15 e^-	19 e^-	24 e^-	29 e^-
–13.5	0.044	0.061	0.050	0.049	0.042	0.040
–13.0	0.052	0.067	0.057	0.056	0.048	0.043
–12.5	0.058	0.074	0.068	0.066	0.061	0.046
–12.0	0.066	0.089	0.092	0.084	0.073	0.066
–11.5	0.085	0.097	0.096	0.088	0.076	0.074
–11.0	0.121	0.121	0.120	0.118	0.102	0.096
–10.5	0.147	0.148	0.145	0.135	0.124	0.116
–10.0	0.177	0.187	0.178	0.164	0.151	0.134
–9.5	0.253	0.255	0.219	0.191	0.176	0.157
–9.0	0.327	0.297	0.259	0.228	0.210	0.181
–8.5	0.462	0.362	0.311	0.267	0.239	0.210
–8.0	0.671	0.435	0.356	0.321	0.270	0.224
–7.5	0.950	0.529	0.441	0.366	0.321	0.272
–7.0	1.057	0.634	0.515	0.453	0.364	0.295
–6.5	1.200	0.740	0.610	0.508	0.500	0.350
-6.0	1.373	0.830	0.675	0.600	0.550	0.390
–5.5	1.410	0.890	0.760	0.650	0.633	0.410
–5.0	1.510	0.990	0.860	0.693	0.666	0.435
–4.5	1.610	0.090	0.960	0.770	0.700	0.461
–4.0	1.760	1.440	1.210	0.949	0.799	0.490
–3.5	2.250	1.790	1.660	1.128	0.931	0.513

Table 8: The final table values for the astrometric correction, $\Delta y(m_{true}, s)$, in pixels. Table values correspond to 2000 parallel shifts for epoch 2020.98.

TRUE m_{inst}	ASTROMETRIC SHIFT (Δy, in pixels)					
	4 e^-	10 e^-	15 e^-	19 e^-	24 e^-	29 e^-
–13.5	0.035	0.033	0.031	0.029	0.027	0.025
–13.0	0.038	0.036	0.034	0.032	0.030	0.028
–12.5	0.047	0.046	0.043	0.042	0.039	0.038
–12.0	0.062	0.062	0.056	0.055	0.053	0.051
–11.5	0.082	0.080	0.071	0.070	0.069	0.065
–11.0	0.113	0.111	0.097	0.093	0.090	0.084
–10.5	0.138	0.138	0.120	0.117	0.112	0.106
–10.0	0.188	0.172	0.145	0.143	0.136	0.127
–9.5	0.261	0.225	0.181	0.173	0.162	0.150
–9.0	0.329	0.278	0.213	0.201	0.189	0.172
–8.5	0.409	0.326	0.247	0.232	0.213	0.192
–8.0	0.504	0.384	0.286	0.263	0.238	0.214
–7.5	0.611	0.446	0.327	0.305	0.263	0.238
–7.0	0.740	0.511	0.371	0.330	0.291	0.257
–6.5	0.870	0.570	0.420	0.357	0.323	0.275
–6.0	0.960	0.630	0.470	0.390	0.357	0.295

7 Conclusions

We have analyzed recent data taken with WFC3/UVIS and extracted trends to characterize the photometric and astrometric losses, distilling the results as a function of background sky value and true flux into two-dimensional tables. We describe how to use these tables to correct photometric and astrometric measurements in WFC3/UVIS `_flt` images.

The CAL-16401 dataset that was used to specify the tables was taken deliberately to help pin down the photometric and astrometric losses. These data were almost perfect for this goal. The distribution of stars in the central ω Cen field was uniform and dense enough to give us many stars to examine the trends.

The backgrounds probed range from 4 electrons to 29 electrons, spaced roughly every 5 e^-. In the future, it may be good to explore higher backgrounds so the correction can be constructed for backgrounds up to ~100 e^-, which can be typical of deep WFC3/UVIS images of galaxies. Perhaps additional probes at 40 e^-, 50 e^-, 75 e^- and 100 e^- might be appropriate.

One of the challenges in making these measurements involved the astrometric correction for the brightest stars. In the future, if we shift the field vertically slightly from chip-stepped pair to the next chip-stepped pair, we can better examine the astrometric shift across the chip gap. That way, we would not have to hope for overlapping observations from the archive. Such a strategy should not have an impact on the other results and should not require any additional exposure time.

Finally, one could also take similar data to evaluate CTE flux losses and astrometric shifts in the *x* direction (from transfer within the serial register). This has been examined before in Anderson (2013), but it would be good to tabulate the current level of losses/shifts so that we can construct a correction.

Acknowledgements

I am grateful to Vera Kozhurina-Platais for her many insightful comments and suggestions, which improved this report considerably. I also appreciate the comments provided by Ben Kuhn and Joel Green on a pre-review draft.

References

Anderson, J. & King, I. R. 2003 AJ 126 772. *The Rotation of the Globular Cluster 47 Tuc in the Plane of the Sky*

Anderson, J. 2014 WFC3/ISR 2014-02. *The Impact of x-CTE in the WFC3/UVIS Detector*

Anderson, J., Baggett, S., & Kuhn, B. 2021 WFC3 ISR 2021-09. *Updating the WFC3/UVIS CTE Model and Mitigation Strategies*

Anderson, J. 2021 WFC3 ISR 2021-TBD. *One-Pass HST Photometry with hst1pass*

Kalirai, J. S. et al. 2012 AJ 143 11. *A Deep, Wide-Field, and Panchromatic View of 47 Tuc and the SMC with HST: Observations and Data-Analysis Methods*

Kozhurina-Platais, V. 2007 ACS/ISR 2007-04. *ACS/WFC: Differential CTE Corrections for Photometry and Astrometry from Non-Drizzled Images*

Kuhn, B. & Anderson, J. 2021 WFC3 ISR 2021-06. *WFC3/UVIS: New flc External CTE Monitoring 2009 - 2020*